J Mater Sci (2011) 46:7815–7821
DOI 10.1007/s10853-011-5762-7

Ion conduction in vanadium-substituted $LiSn_2P_3O_{12}$ electrolyte nanomaterials

R. Norhaniza · R. H. Y. Subban · N. S. Mohamed

Received: 27 January 2011 / Accepted: 30 June 2011 / Published online: 13 July 2011

Abstract $LiSn_2P_{3-y}V_yO_{12}$ powders with $y = 0.2$, 0.4, 0.6, and 0.8 are prepared by mechanochemical milling method. The pellets of the compounds are heat treated at temperatures between 700 to 1,000 °C for sintering period of 8 h. X-ray diffraction analysis indicates that all samples consist of rhombohedral crystalline $LiSn_2P_3O_{12}$ phase. Energy dispersive X-ray analysis confirmed that V^{5+} has been successfully substituted into $LiSn_2P_3O_{12}$ crystalline phase. The conductivities of the pellets are determined using impedance spectroscopy. Impedance analysis shows enhancement in both bulk and grain boundary conductivities with increase in y. The enhancement in bulk conductivity is due to decrease in bulk activation energy reflecting an increase in ion mobility as a result of an increase in bottleneck size. Enhancement in grain boundary conductivity is attributed to increase in the number of conducting pathways due to an increase in crystallite homogeneity.

R. Norhaniza (✉)
Institute of Graduate Studies, University of Malaya,
50603 Kuala Lumpur, Malaysia
e-mail: r.norhaniza@ymail.com

R. H. Y. Subban
Faculty of Applied Sciences, Universiti Teknologi MARA,
40450 Selangor, Malaysia
e-mail: rihanum43@salam.uitm.edu.my

N. S. Mohamed
Centre for Foundation Studies in Science, University of Malaya,
50603 Kuala Lumpur, Malaysia
e-mail: nsabirin@um.edu.my

Introduction

Polycrystalline materials with sodium super ionic conductor (NASICON) structure exhibit high ionic-conducting capabilities due to existence of three dimension, 3D, conduction pathways which enables easy migration of mobile ions [1–4]. $LiSn_2(PO_4)_3$ is one of the compounds that possess structure analogous to NASICON structure. The basic structure of $LiSn_2(PO_4)_3$ is rhombohedral. This basic structure consists of a three dimensional framework of two SnO_6 octahedra sharing corner oxygens of PO_4 tetrahedra forming $[Sn_2(PO_4)_3]^-$. This framework is covalently bonded making it highly stable with high melting point of above 1,650 °C [3]. In the $[Sn_2(PO_4)_3]^-$ skeleton, each SnO_6 octahedron is separated by three PO_4 tetrahedra and each of this PO_4 tetrahedra is connected to four SnO_6 octahedra [2]. This skeleton in turn forms chain like "ribbons" along the *c*-axis. The ribbons are joined together along the *a*- and *b*- axis by PO_4 tetrahedra. The corner sharing of oxygen ions between the SnO_6 octahedra and PO_4 tetrahedra results in an open framework structure with structural holes. These structural holes give some freedom for rotational motion to the structure. This flexibility allows substitution of various ions at Sn and P sites. $LiSn_2(PO_4)_3$ framework consists of two types of sites that can be occupied by lithium ions: (i) M_1 sites located between SnO_6 octahedral are sites that have six coordination with oxygens forming LiO_6 octahedra and (ii) M_2 sites, located between the ribbons of PO_4 tetrahedra has a distorted eight coordination with oxygens. Both sites are arranged in an alternating form of a 3D array along conduction channels, also known as bottlenecks, which allow transportation of cations [1–6].

A few researchers have reported studies on $LiSn_2P_3O_{12}$ prepared via solid state reaction [7, 8]. However, their

$LiSn_2P_3O_{12}$ pellets showed low conductivities in the order of 10^{-10} S cm^{-1} due to the presence of Teflon which was used as a binding agent to avoid pellets from breaking during characterization. Recently, the authors have reported stable pellets of $LiSn_2P_3O_{12}$ prepared by mechanochemical milling method without the use of any binder [9]. These pellets showed conductivity values in the order of 10^{-7} S cm^{-1} which are higher than those reported in references [7, 8]. The focus of this work is to prepare vanadium-substituted V^{5+} into $LiSn_2P_3O_{12}$ to form compounds with a general formula of $LiSn_2(PO_4)_{3-y}(VO_4)_y$ with the hope of enhancing conductivity. The compositional effects on the conductivity of the compounds as well as their structure are investigated.

Experimental

Stoichiometric proportions of Li_2O (99%, Aldrich), SnO_2 (98%, Sigma-Aldrich), $NH_4H_2PO_4$ (98%, Sigma-Aldrich), and V_2O_5 (98%, Aldrich) were prepared according to the formula $LiSn_2P_{3-y}V_yO_{12}$ ($y = 0.2$, 0.4, 0.6, and 0.8) and heated at 700 °C for 2 h. This heating process was done to decompose the hydrogen phosphate and initiate its reaction with the carbonate during heating [8, 10]. After heating process, the mixtures were milled for 80 h using Fristch 7 planetary ball mill. Milled powders were then pelletized to form pellets with diameter of 13 mm using a hydraulic press at a pressure of 7 ton. The pellets were then sintered at four different temperatures, T from 700 to 1,000 °C for 8 h. It was observed that different y values exhibit optimum conductivity at different sintering temperatures which were at 700 and 600 °C for $y = 0.2$ and 0.4, respectively, while for $y = 0.6$ and 0.8, the optimum sintering temperature was 500 °C. For further analysis samples were prepared by sintering them at their optimized sintering temperatures and these samples are labeled as V2, V4, V6, and V8 for y of 0.2, 0.4, 0.6, and 0.8, respectively.

Impedances of samples were measured using Solartron SI 1260 impedance analyzer while X-ray diffraction (XRD) data of the samples were recorded using Bruker D8 Advance X-Ray Diffractometer. To study crystallite size, Scherer equation was applied [11];

$$D = \frac{k\lambda}{\beta \cos\theta} \quad (1)$$

where k is the Scherer constant value (0.94), λ is the wavelength of the source (1.5406 Å), β is FWHM (in radians), and θ is the Bragg angle (in radians). Quanta 200 FESEM scanning electron morphology (SEM) equipment interfaced with energy dispersive X-ray (EDX) instrument was used for microstructure and elemental composition analyses. Transference numbers were analyzed by Wagner's polarization method using Solartron SI 1287 Electrochemical Interface in order to determine the type of charge carrier in the samples.

Results and discussion

The X-ray diffraction spectra for V2 to V8 are depicted in Fig. 1. The spectra clearly indicate the presence of rhombohedral $LiSn_2(PO_4)_3$ crystalline phase (label with miller indices of plane) in the samples. This phase has lattice parameters; $a = 8.650$ Å, $b = 8.650$ Å, and $c = 21.487$ Å. These parameters are same with the parameters obtained for $LiSn_2P_3O_{12}$ systems reported in [9] showing that the vanadium-substituted samples have the same crystalline phase as that of the $LiSn_2(PO_4)_3$ parent compound. SnO_2 impurity is also observed in all samples indicating the presence of unreacted SnO_2. However, no peak attributed to vanadium-related compounds is observed. Therefore, it can be inferred that vanadium has been successfully substituted into $LiSn_2(PO_4)_3$ crystalline matrix. Figure 2 shows the comparison of crystallite size for all samples. All samples are found to have crystallite sizes in the order of 10^{-9} m indicating that they are nano in size. The distribution of crystallite size in each sample is almost the same at all planes except for plane 300 especially for samples V2 and V4. This indicates that samples V6 and V8 have crystallites which are homogenous while those of V2 and V4 contain crystallites of smaller sizes in between larger crystallites.

Figure 3 shows micrograph images of the morphology for the cross-section surface of V2, V4, V6, and V8. V2 shows some agglomeration of grains of different sizes. In V4, the agglomerations are of smaller sizes and more homogeneous

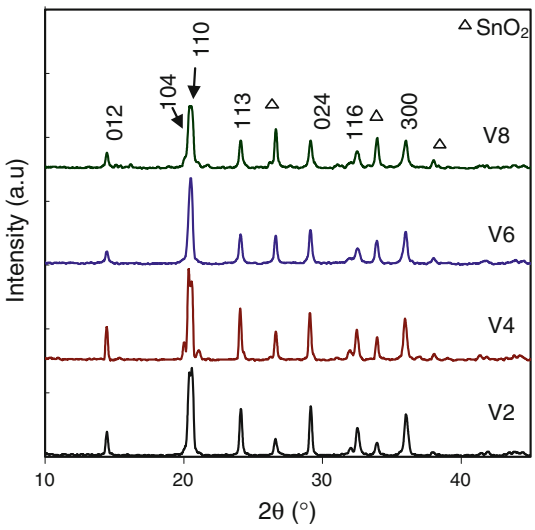

Fig. 1 X-ray diffraction patterns for V2, V4, V6 and V8

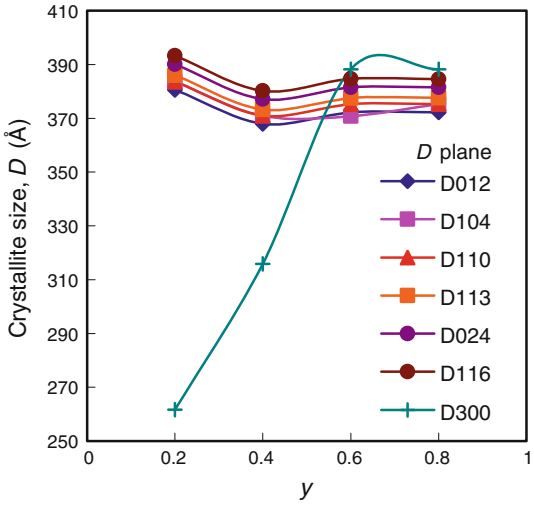

Fig. 2 Variation of crystallite size with y (vanadium content) at different planes

compared to V2. V6 and V8 show crystallites of about the same size which is in agreement with the results of crystallite size analysis presented in Fig. 2. In V6, agglomerations of grains are also observed. In addition, needle-like structures are also found scattered between these agglomerations.

Figure 4 shows EDX spectra for V2, V4, V6, and V8. The details of the EDX spectra analysis are tabulated in Table 1. As lithium is not detectable by EDX due to its light atomic weight which does not permit the analysis of emitted radiations, the concept of charge neutrality is applied [12]. It is found that the ratios of the elements in the compounds are in good agreement with the stoichiometric ratio of the starting materials. This analysis confirms that vanadium has been successfully substituted at P sites in $LiSn_2P_3O_{12}$ matrix. This supports the XRD results discussed earlier. From the table, it can also be observed that the needle-like structures contain high percentage of vanadium. However, this compound is expected to exist in small amounts as it is not detectable by XRD. Structure of SnO_2 observed in XRD is not detected in SEM micrographs. This compound is believed to be present in other spots or parts in the samples which are not shown in Fig. 3.

A typical impedance plot for the studied compounds is displayed in Fig. 5. The figure shows two overlapping semicircles followed by a spike in the low frequency region. The high frequency semicircle is assigned to bulk response with its intercept at the x-axis assigned to bulk resistance, R_b, while the middle frequency semicircle is assigned to grain boundary response with its intercept at the x-axis corresponds

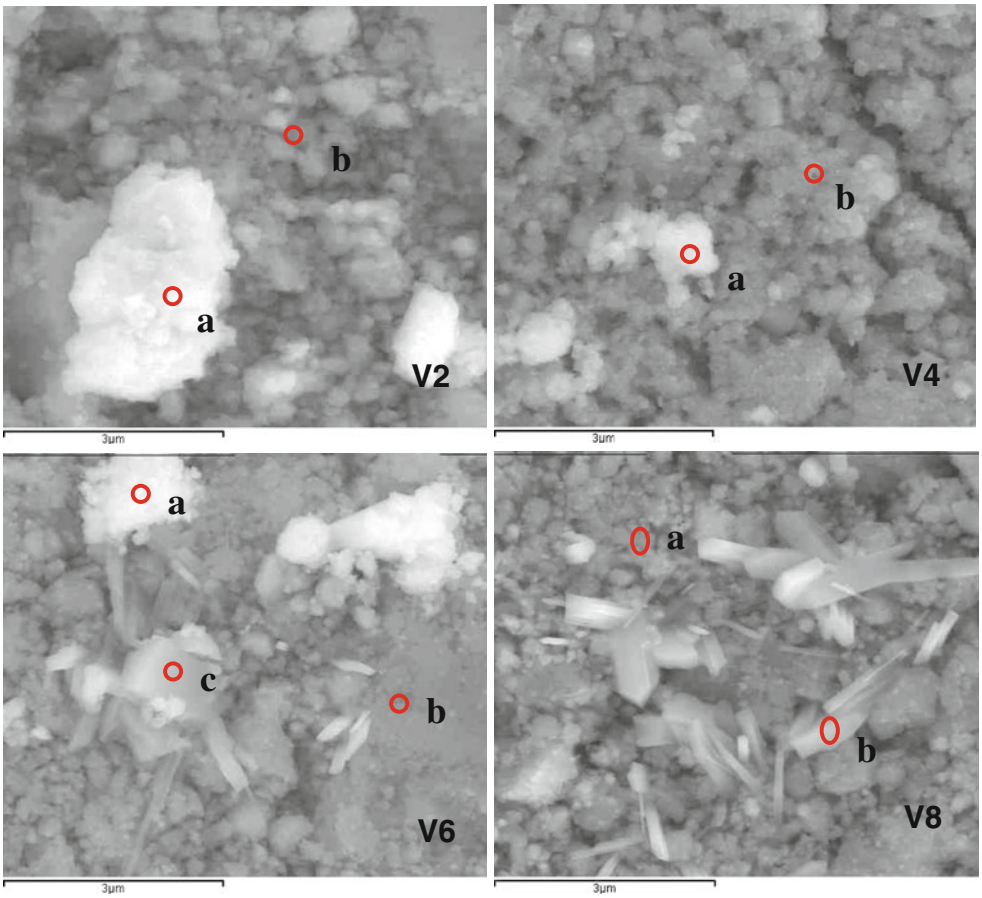

Fig. 3 SEM micrographs of V2, V4, V6, and V8

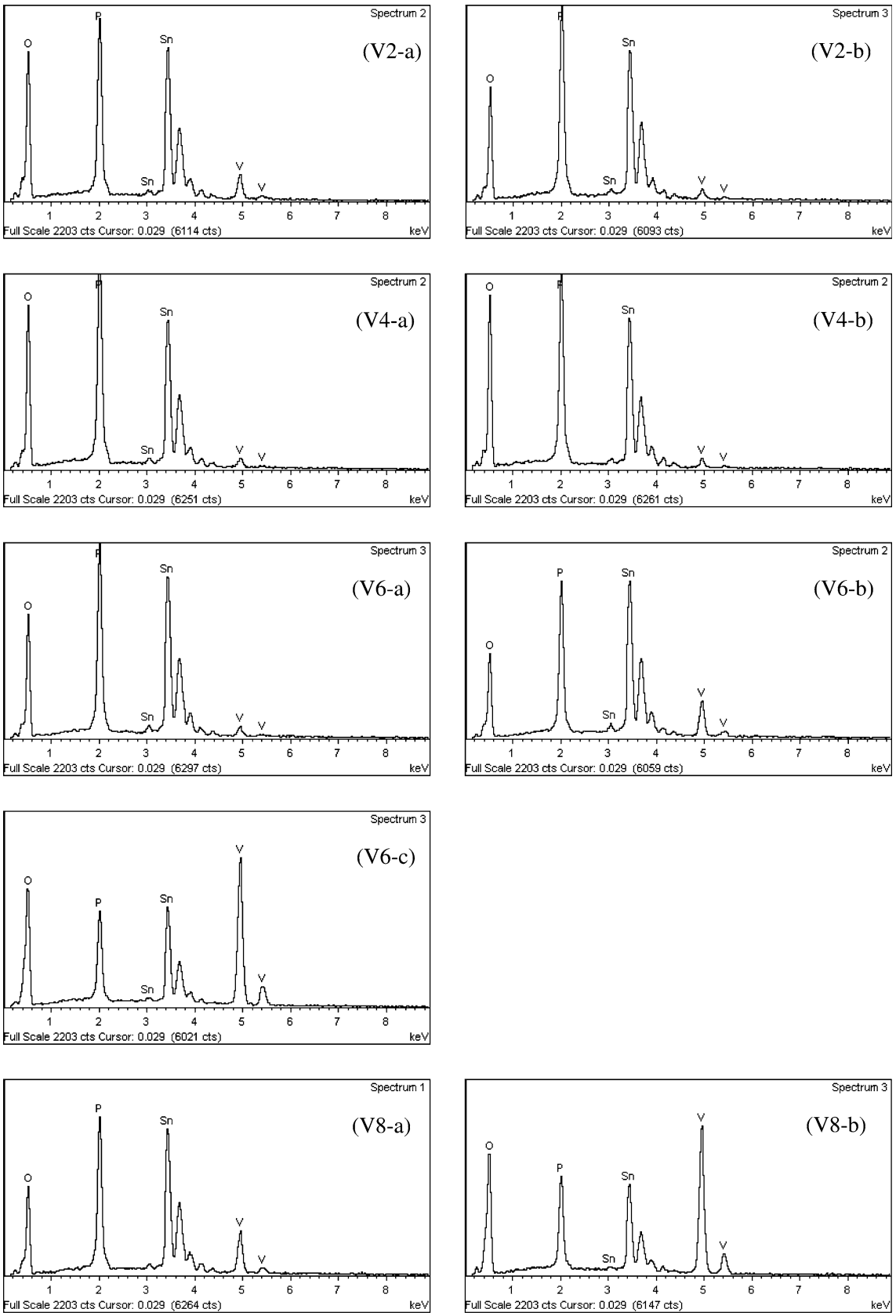

Fig. 4 EDX spectra at each points a, b, and c for all samples

Table 1 Atomic percentage of elements at each point for all samples

Sample	Composition	Stoichiometric ratio Sn:P:V
V2	Starting mixture	2.0:2.8:0.2
	Fig. 4 V2-a	2.00:2.79:0.19
	Fig. 4 V2-b	2.00:2.78:0.20
V4	Starting mixture	2.0:2.6:0.4
	Fig. 4 V4-a	2.00:2.56:0.41
	Fig. 4 V4-b	2.00:2.51:0.38
V6	Starting mixture	2.0:2.4:0.6
	Fig. 4 V6-a	2.00:2.35:0.61
	Fig. 4 V6-b	2.00:2.42:0.55
	Fig. 4 V6-c	1.00:1.28:2.94
V8	Starting mixture	2.0:2.2:0.8
	Fig. 4 V8-a	2.00:2.16:0.79
	Fig. 4 V8-b	1.00:1.22:2.90

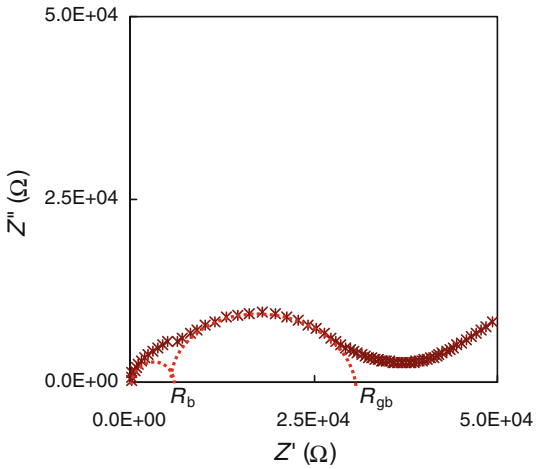

Fig. 5 Impedance plot for V2

to grain boundary resistance, R_{gb}. Bulk and grain boundary conductivities, σ_b and σ_{gb} are calculated using R_b and R_{gb} values determined from the impedance plots.

To confirm the conductivity obtained from the impedance plots, conductivity spectra (imaginary part of conductivity, σ'' vs. real part of conductivity, σ') are plotted and a typical spectrum is shown in Fig. 6. The conductivity plot consists of a semicircle and two dispersion curves at low σ' and high σ' regions, respectively. The intercept of the dispersion curves with x-axis at high and middle frequency gives the values of σ_b and σ_t (total conductivity), respectively. This method has been used by a few groups of researchers [13–16]. The σ_{gb} is obtained by subtracting σ_b from σ_t. The conductivities were then compared with the conductivity values obtained from the impedance plots and these values are found to be in good agreement with each other as listed in Table 2.

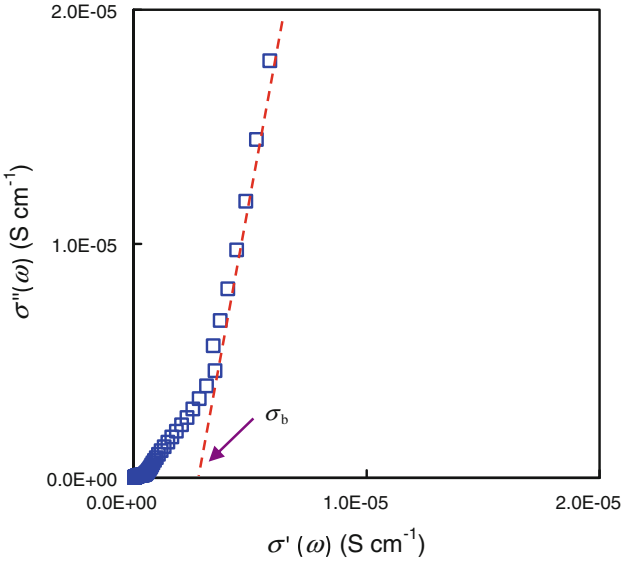

Fig. 6 Conductivity spectrum for V2

Table 2 Comparison of conductivity values determined from impedance and conductivity plots for all samples

Sample	$\sigma_b \times 10^{-6}$ (S cm^{-1})		$\sigma_{gb} \times 10^{-6}$ (S cm^{-1})	
	Z plot	σ plot	Z plot	σ plot
V2	3.77 (±0.01)	3.76 (±0.03)	0.67 (±0.01)	0.65 (±0.01)
V4	4.81 (±0.03)	4.79 (±0.03)	1.51 (±0.02)	1.53 (±0.02)
V6	5.37 (±0.01)	5.40 (±0.03)	2.61 (±0.03)	2.61 (±0.01)
V8	5.70 (±0.02)	5.71 (±0.01)	2.71 (±0.01)	2.71 (±0.01)

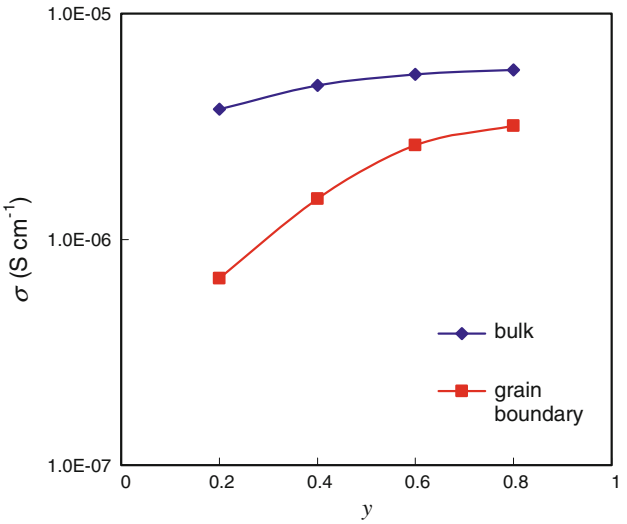

Fig. 7 Conductivity variations with y for $LiSn_2P_{3-y}V_yO_{12}$ system

Figure 7 illustrates variations of bulk and grain boundary conductivities with vanadium content. As seen in the figure, both conductivities are observed to increase with

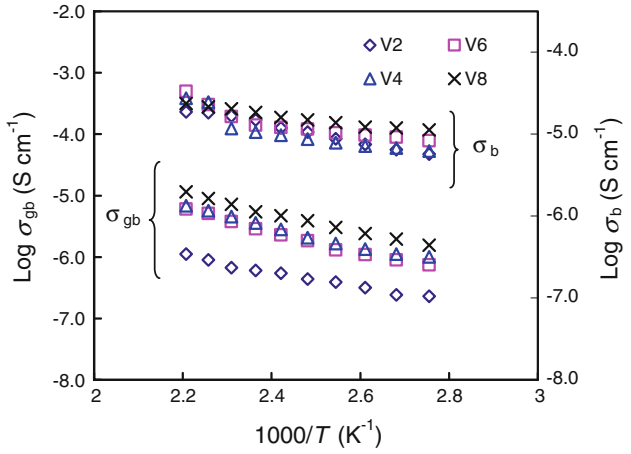

Fig. 8 Temperature dependence of conductivity for $LiSn_2P_{3-y}V_yO_{12}$ system

Table 3 Bulk and grain boundary activation energies for all samples

Sample	$E_{a,b}$ (eV)	$E_{a,gb}$ (eV)
V2	0.17	0.30
V4	0.16	0.29
V6	0.14	0.30
V8	0.12	0.29

increase in vanadium content. V8 exhibits the highest conductivity with values of σ_b and σ_{gb} of 5.70×10^{-6} and 2.71×10^{-6} S cm^{-1}, respectively. This means that σ_b is increased by about four times while σ_{gb} shows an enhancement of one order of magnitude compared to σ_b and σ_{gb} of the $LiSn_2(PO_4)_3$ parent compound which are 1.65×10^{-6} and 1.05×10^{-7} S cm^{-1}, respectively [9].

Conductivity–temperature dependence of all samples is studied in the temperature range 353 to 463 K and the plots of log σ versus 1,000/T are shown in Fig. 8. It is observed that the bulk conductivity for all samples increases with temperature. All samples show linear log σ versus 1,000/T plots with regression values of around 0.98 and 0.99 for both σ_b and σ_{gb}, respectively. As such, it can be inferred that the conductivity is Arrhenian in nature. However, a sudden increase in σ_b is detected at around 170 °C for V4 and V6 which is believed to be associated with a change in crystalline phase [17]. The activation energy values, E_a were calculated from the Arrhenius slope and these are listed in Table 3. It is found that bulk activation energy, $E_{a,b}$ decreases with increase in vanadium content. V8 shows the lowest value of 0.12 eV. This value is smaller compared to E_a reported by Juarez et al. [7, 18] and Winand et al. [19] which are 0.34 and 0.55 eV, respectively. The decrease in activation energy reflects greater ion mobility which maybe due to an increase in bottleneck size in the structure [20, 21]. A similar observation has been reported by Chang et al. [21]. These authors reported that partial substitution of P^{5+} ions by V^{5+} ions in $Li_{1.3}Al_{0.3}Ti_{1.7}(PO_4)_3$ led to conductivity enhancement attributed to change in bottleneck size. In the system studied in the present work, $(PO_4)^{3-}$ tetrahedral is partially substituted by the larger $(VO_4)^{3-}$ forming larger bottlenecks leading to greater mobility of ions which in turn enhance conductivity [20, 21]. The increase in V content increases the bottleneck size leading to an increase in conductivity as shown in Fig. 7. In the case of grain boundary activation energy, $E_{a,gb}$, all samples show similar values indicating no significant effect of vanadium content on the $E_{a,gb}$. The increase in σ_{gb} with vanadium content maybe due to increase in the number of conducting pathways as a result of increase in contact surface area between grains as a result of increase in homogeneity of crystallites with increase in V content as presented in Fig. 2 [22, 23]. According to Kawai and Kuwano [24], σ_{gb} affects the ionic transportation in the bulk property. Thus, when σ_{gb} increase, the σ_b also increase as observed before.

The increase in the conductivity with vanadium content may also be attributed to increase in polarizability of cation–oxygen bond which formed the bottlenecks. According to Chowdari et al. [25] and Sugantha and Varadaraju [26], the larger the polarizability of cation-oxygen bond, the

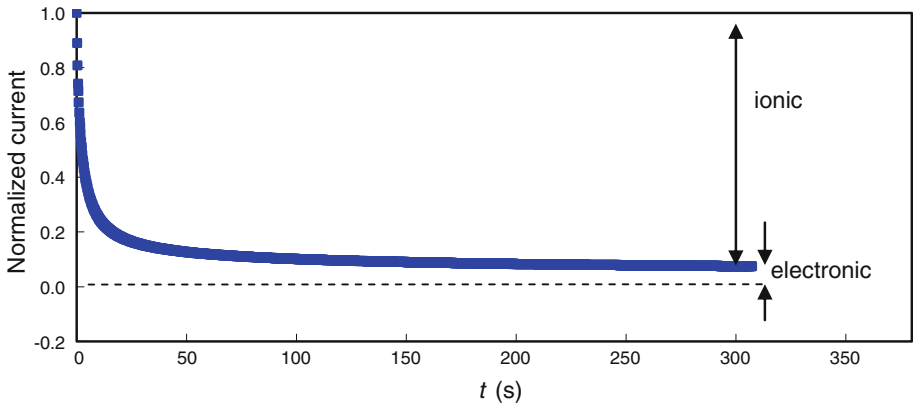

Fig. 9 Normalized current versus time for V2

easier the transport of ions in the bottleneck. Therefore, increase in vanadium increased the ion transportation which results in increase in conductivity.

Ionic transference number is the ratio of ionic conductivity to the total conductivity which is ionic and electronic. In this study, the ionic transference number is measured by Wagner's polarization method. Figure 9 presents a typical direct current polarization curve. Similar result obtains for all samples. The values of the transference numbers are 0.98, 0.98, 0.95, and 0.93 for V2, V4, V6, and V8, respectively. Since the transference numbers are close to unity, it can be inferred that the majority mobile charge carriers are ions and they are expected to be Li^+. These values also indicate that there is a small electronic contribution associated with SnO_2 present in the samples as shown by XRD spectra in Fig. 1.

Conclusion

Partial substitution of V^{5+} in P^{5+} sites resulted in enhancement of bulk and grain boundary conductivities. Enhancement in bulk conductivity is due to increase in bottleneck size by partial substitution of vanadium which is reflected by a decreases in $E_{a,b}$. Increase in σ_{gb} with vanadium content is attributable to increase in number of conducting pathways as a result of increase in homogeneity of crystallites.

References

1. Goodenough JB, Hong HYP, Kafalas JA (1976) Mater Res Bull 11:203
2. Leo CJ, Chowdari BVR, Rao GVS, Souquet JL (2002) Mater Res Bull 37:1419
3. Kumar PP, Yashonath S (2006) J Chem Sci 118:135
4. Taoufik I, Haddad M, Brochu R, Berger R (1999) J Mater Sci 34:2943. doi:10.1023/A:1016064913446
5. Berry FJ, Costantini N, Smart LE (2006) Solid State Ionics 177:2889
6. Anantharamulu N, Rao KK, Rambabu G, Kumar BV, Radha V, Vithal M (2011) J Mater Sci 46:2821. doi:10.1007/s10853-011-5302-5
7. Juarez AM, Jimenez R, Martin PD, Ibanez J, Rojo JM (1997) J Phys Condens Matter 9:4119
8. Lazarraga MG, Ibañez J, Tabellout M, Rojo JM (2004) Compos Sci Technol 64(5):759
9. Norhaniza R, Subban RHY, Mohamed NS (2010) Adv Mater Res 129–131:338
10. Ward BJ, Liu CC, Hunter GW (2003) J Mater Sci 21:4289. doi:10.1023/A:1026374830114
11. Savitha T, Selvasekarapandian S, Ramya CS, Bhuvaneswari MS, Angelo PC (2007) J Mater Sci 42:5470. doi:10.1007/s10853-006-0983-x
12. Aboulaich A, Conte DE, Fourcade JO, Jordy C, Willmann P, Jumas JC (2010) J Power Sources 195:3316
13. Orliukas AF, Dindune A, Kanepe Z, Ronis J, Bagdonas B, Kezionis A (2006) Electrochim Acta 51:6194
14. Sobiestianskas R, Dindune A, Kanepe Z, Ronis J, Kezionis A, Kazakevicius E, Orliukas A (2000) Mater Sci Eng B 76:184
15. Cretin M, Fabry P (1999) J Eur Ceram Soc 19:2931
16. Godichemeier M, Michel B, Orliukas A, Bohac P, Sasaki K, Gauckler L, Heinrich H, Schwander P, Kostorz G, Hofmann H, Frei O (1994) J Mater Res 9:1228
17. Koteswara KR, Rambabu G, Raghavender M, Prasad G, Kumar GS, Vithal M (2005) Solid State Ionics 176:2701
18. Juarez AM, Pecharroman C, Iglesias JE, Rojo JM (1998) J Phys Chem 102:372
19. Winand JM, Rulmont A, Tarte P (1991) J Solid State Chem 93:341
20. Best AS, Newman PJ, MacFarlane DR, Nairn KM, Wong S, Forsyth M (1999) Solid State Ionics 126:191
21. Chang CM, Lee Y, Hong SH (2005) J Am Ceram Soc 88(7):1803
22. Fu J (1997) Solid State Ionics 104:191
23. Mei A, Jiang QH, Lin YH, Nan CW (2009) J Alloys Compd 486:871
24. Kawai H, Kuwano J (1994) J Electrochem Soc L78:141
25. Chowdari BVR, Radhakrishnan K, Thomas KA, Subba Rao GVL (1989) Mater Res Bull 24(2):221
26. Sugantha M, Varadaraju UV (1997) Solid State Ionics 95:201